Faults and ground uplift at active calderas

A. FOLCH[1] & J. GOTTSMANN[2,3]

[1]*Istituto Nazionale di Geofisica e Vulcanologia – Sezione Osservatorio Vesuviano, Via Diocleziano 326, 80124 Naples, Italy*

[2]*Institute of Earth Sciences, Jaume Almera, IJA-CSIC, Lluís Solé Sabarís s/n, 08028 Barcelona, Spain*

[3]*Department of Earth Sciences, University of Bristol, Wills Memorial Building, Queens Road, Bristol BS8 1RJ, UK (e-mail: j.gottsmann@bristol.ac.uk)*

Abstract: Subsurface volume and pressure increases triggering surface inflation at active calderas are generally deduced by inverting ground-deformation time-series using isotropic and homogeneous half-space models (IHM). These models represent simplified mathematical analogues of the mechanical behaviour of the Earth's crust. Using three-dimensional numerical modelling, we show that lateral discontinuities such as intracaldera- or caldera-ring-faults can significantly amplify and distort the ground deformation pattern during unrest. As a consequence, data inversions using IHMs, which do not consider lateral discontinuities, can provide erroneous results on causative source parameters. We also find that the degree of amplification and distortion in the form of abrupt changes in displacement/distance gradients in proximity to faults is dependent on source geometry. Prolate bodies represent a particularly critical geometry for which pressure increases may be overestimated by a factor of up to three. Our 3D analysis suggests that amplification effects can be much larger than predicted by earlier 2D models. We validate theoretical results by applying our model to investigate the effect of boundary faults and source geometries on the displacement field during ground uplift at the restless calderas of Campi Flegrei (Italy) and Sierra Negra (Galapagos Islands, Ecuador). Based on the discrepancy in results from IHMs and our numerical model, we argue that employing IHMs for inversion of ground displacement and gravity time-series may in some cases lead to a biased assessment of hazards associated with ground uplift.

Volcanic calderas are (sub)circular surface depressions of up to tens of kilometres in diameter and of up to several hundred metres in topographic change from rim to floor. Calderas are thought to be formed by slip along boundary faults as a result of gravitational collapse of overlying rocks into an emptying reservoir during large-scale volcanic eruptions (Lipman 2000). Many calderas undergo episodes of unrest associated with seismicity and/or ground deformation (Newhall & Dzurisin 1988). Periods of ground inflation are of particular interest for volcanic hazard assessment. Inflation is generally interpreted to result from a subsurface volume and pressure increase, which may be caused by a number of processes. Among those, replenishment of magma into an existing reservoir is a key candidate (Battaglia *et al.* 1999), and also a potential trigger for volcanic eruptions (Murphy *et al.* 1998). Alternatively, volume/pressure increases within a subsurface hydrothermal system may equally well account for significant ground deformation (Bonafede & Mazzanti 1998). Unrest culminating in the renewal of volcanic activity at a caldera in a densely populated area, such as, for example, Campi Flegrei (Italy), will cause significant socio-economic disruption for local communities and beyond, and it is therefore important to assess the nature of the source that causes the unrest, in order to assess hazards and mitigate risks.

A widely applied technique to quantify subsurface volume/pressure changes is the inversion of ground deformation data time-series. Point (Mogi 1958; McTigue 1987) or extended (Davis 1986; McTigue 1987; Yang *et al.* 1988; Fialko *et al.* 2001) pressure sources embedded within an elastic or anelastic medium (Dragoni & Magnanensi 1989; Bonafede 1990; Hofton *et al.* 1995; Fernandez *et al.* 1997) under certain assumptions will permit analytical solutions. Simplified physical models that have analytical solutions (e.g. the Mogi model) are extremely popular and enormously facilitate the solution of the inverse problem. However, there is evidence that surface deformation at active calderas is

From: TROISE, C., DE NATALE, G. & KILBURN, C. R. J. (eds) 2006. *Mechanisms of Activity and Unrest at Large Calderas*. Geological Society, London, Special Publications, **269**, 109–120.
0305-8719/06/$15.00

likely to be strongly influenced by the presence of faults and discontinuities (De Natale & Pingue 1993; De Natale *et al.* 1997; Beauducel *et al.* 2004), which are not considered by isotropic and homogeneous half-space models (IHM). One may conclude that the spatial distribution of the deformation field at caldera-type volcanoes is limited by the presence of caldera boundary faults. The motivation for this study lies in our recognition of the often unrealistic parameters obtained from inversion for 'simple' analytical models, even though their synthetic deformation data show an excellent fit to the observed data. In this framework, the omission of lateral medium discontinuities in the inverse problem may cause significant misfits leading to unrealistic values for source parameters such as the associated pressure change.

This paper is organized into two parts: the first part provides a parametric study of the influence of faults on the surface deformation pattern. Results can be viewed as an extension of previous studies (De Natale & Pingue 1993) to 3D geometries. In the second part, we investigate the interaction of caldera boundary faults with the displacement field at two recently uplifting caldera volcanoes, the Campi Flegrei Caldera, Italy, and the Sierra Negra Caldera, Ecuador. Our results have important consequences for geodetic data inversion and its contribution to hazard assessment and risk mitigation in areas undergoing ground deformation during caldera unrest.

Caldera faults and modelling framework

We will limit our investigation to ground uplift resulting from a subsurface volume/pressure increase. From the perspective of hazard assessment, this scenario has the greatest potential to provide unrealistic results for subsurface kinetics from analytical data inversion if oversimplifications in the modelling framework are not accounted for. In this study we are concerned with a volume/pressure increase beneath the caldera floor, which is bounded by either ring-faults that represent the structural margins of a caldera (Gudmundsson *et al.* 1997; Acocella *et al.* 2000) or by intracaldera structural discontinuities that dissect the floor into individual blocks (Orsi *et al.* 1996). In either case, field and geophysical investigations suggest that fault inclination is generally subvertical to vertical (Mori & McKee 1987; Orsi *et al.* 1996; Prejean *et al.* 2002). For this study the physical phenomenon responsible for the pressure increase in the source is irrelevant, and can be of either magmatic and/or hydrothermal origin.

Consider the scenario depicted in Figure 1. A source of dilatation undergoing pressure changes is embedded in a fractured medium. The model geometry can be characterized in terms of two dimensionless scaling quantities, ε and ξ_f. The former is the ratio of source depth d (measured from the surface to the top of the source) to its horizontal extension a ($\varepsilon = d/a$). Depending on

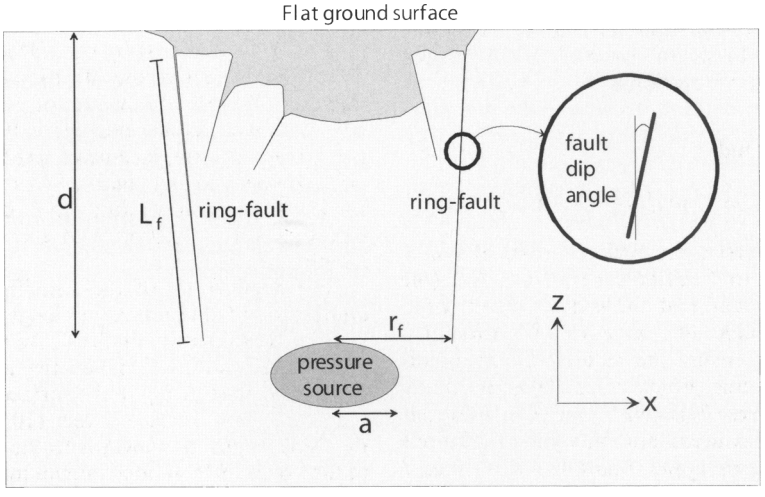

Fig. 1. Sketch of the model. A pressure source of characteristic horizontal extension a and depth d is embedded within a fractured linear elastic medium. Ring-faults (or intracaldera structural discontinuities) of averaged length L_f and dip angle α are located at a distance r_f from the source centre. Faults may start at variable depths and extend downwards to the top of the pressure source.

the geometry being considered, a represents the source radius (spherical source), the semi-major axis (oblate spheroid), or the semi-minor axes (prolate spheroid). The latter dimensionless number is expressed as the ratio of the distance between the centre of the source and the tip of the fault r_f to a ($\xi_f = r_f/a$). We will assume axial symmetry – a reasonable hypothesis in the context of collapse calderas – and a flat free surface located at $z = d = 0$. Equations of linear elasticity have been solved numerically via a finite-element method with nodal implementation (Codina & Folch 2004) for different source geometries and combinations of the scaling parameters, fault dip angle α, and fault lengths L_f. The fault lengths are chosen such that they extend from various depths downwards to a penetration depth equal to d; i.e. they extend to depths equal to that of the top of the source. As a consequence, we can explore the effect of the presence of caldera-fill successions overlying the fractured medium on the deformation field. Boundary conditions imposed at faults are zero shear strength (corresponding to null friction) and the non-overlapping condition (De Natale & Pingue 1993).

The effect of the presence of faults on the intracaldera deformation field is compared to the predictions of the maximum displacements (U_z^* for vertical and U_r^* for horizontal) obtained from applying an IHM. The purpose of this normalization is twofold. First, it allows an immediate estimation of the error incurred by applying an IHM to model mechanical behaviour in faulted environments. Second, results become independent of source overpressure and the elastic properties of the medium. Standard values for rigidity $\mu = 10$ GPa and Poisson's ratio $\nu = 0.25$ have been assumed in the simulations.

Parametric study

Results for a spherical source (Mogi-type)

We consider first a pressurized spherical source with a equal to 1 km at a depth of 4 km (the depth to the centre of the sphere equals $d+a$; Fig. 2). The values of ε have been fixed to equal 4 in order to ensure the validity of the point-source hypothesis (Folch *et al.* 2000). By doing this, differences between numerical solutions for extended sources and analytical solutions for point source approximations, in this case the Mogi solution (Mogi 1958), become negligible in the absence of faults. As a consequence, any difference between the surface displacements obtained from solutions for the faulted medium and those obtained by the homogeneous

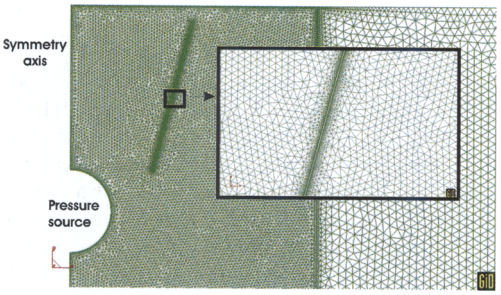

Fig. 2. Details of a finite element mesh. Only a part of the computational domain is shown. The source is represented by a sphere at 4 km depth and has a radius of 1 km ($\varepsilon = 4$). In this example the fault starts at a depth equal to 10% of the source depth (i.e. 400 m) and extends downwards to a depth corresponding to the top of the source. The inset shows a close-up of the mesh close to the fault. For all simulations, meshes have been refined until the precision level of numerical solutions for displacements lies in the range of millimetres.

approaches (numerical solutions considering extended sources or the analytical solution for Mogi point source) must be attributed to the presence of faults. As a consequence, results from this section can be viewed as an estimation of the error in the popular Mogi model when applied in a faulted medium.

Figure 3 illustrates the effect of fault distance on the displacement field. The amplification of deformation becomes less significant with increasing distance between the source and the fault. For instance, for $\xi_f = 2$, the maximum vertical displacement at the surface is almost 2.5 times greater than predicted by the IHM, whereas for $\xi_f = 5$ the maximum amplification becomes less than 10%. Finally, for values of $\xi_f \geq 6$ the influence of faults becomes negligible. Positive deviations from the displacements predicted by the IHM are particularly significant in the near field up to a dimensionless distance ξ equal to $\xi_f + 1$, regardless of the distance to the fault and its length.

The dependence of the amplification of the deformation field on the fault length and vertical location is shown in Figure 4. As expected, the longer the fault the higher the amplification. Faults not penetrating to the surface, but extending from near surface levels (10% or less of the fault length) downwards to the source depth induce over 50% greater maximum vertical displacements than faults nucleating about halfway in-between (Fig. 4a). A similar yet slightly more pronounced amplification of surface deformation is induced by faults extending from the surface downwards to depths between 50 and

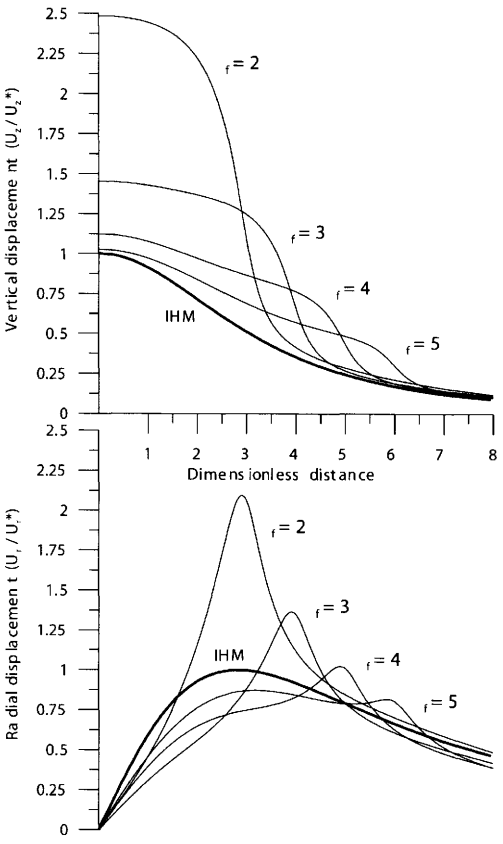

Fig. 3. Effect of fault distance $\xi_f = r_f/a$ on vertical (top) and radial (bottom) displacements. Radial distance from the centre of the source is displayed as the non-dimensional parameter $\xi = r/a$. Results for faults located at distances ξ_f of 2, 3, 4 and 5. Bold lines indicate the predictions of the isotropic, homogeneous half-space model (IHM). Plots are normalized to U_z^* and U_r^*, the maximum vertical and radial displacements, respectively, as obtained from the IHM. Model parameters for these solutions are $a = 1$ km, $d = 4$ km, $\varepsilon = 4$, $\alpha = 15°$ and $L_f = 3725$ m. The distance between the top of the fault and the free surface is 10% of the fault length.

100% of the source depth, as shown in Figure 4b. It follows that, for a fixed fault length, the closer the depth of the tip of the fault matches the source depth, the higher the amplification. Maximum radial displacements are between 1.2 and 2.0 times the maximum radial displacement predicted by the IHM. The lateral distance of the predicted maximum for the investigated fault lengths, however, is in reasonable agreement with that given by the IHM.

The effect of fault inclination on the displacement field is illustrated in Figure 5. Slightly inward-dipping faults ($\alpha > 0$) appear to amplify both vertical and horizontal displacements more than slightly outward-dipping faults ($\alpha < 0$), but they also extend the maximum radial deformation field to significantly larger wavelengths. In contrast, the presence of outward-dipping faults markedly reduces the lateral extent of surface displacements compared to predictions from the IHM.

Effect of source geometry

In addition to the characteristics of the faults, the geometry of the causative source bounded by faults plays a major role in amplifying the displacement field at caldera volcanoes. This effect is likely to be much more pronounced for prolate source geometries than for oblate geometries. Ring-faults are (sub-)vertical discontinuities and, in consequence, their interaction with the stress field produced by pressurizing a prolate source is stronger than by pressurizing an oblate source. This phenomenon is illustrated in Figure 6 for four spheroidal sources with different aspect ratios e (vertical to horizontal extension), including spherical, oblate and prolate geometries. For vertically elongated sources, the amplification can be as high as a factor of four for the vertical component and two for the radial component, when compared to the IHM solutions. In contrast, for horizontally extended sources, the amplification effect decreases progressively with the source aspect ratio. For geometries such as laccoliths or sills (with $e \ll 0.25$) the effect of ring-faults on the deformation field becomes a second-order effect, and concentrates just in the vicinity of the fault projection to the surface.

Discussion

The present study gives insights into the dependence of the surface deformation field at active volcanic calderas on (sub)vertical structural discontinuities. As shown by previous 2D studies (De Natale & Pingue 1993), the presence of faults may alter notably the shape of both vertical and radial deformation patterns, as well as their absolute value. However, our 3D analysis suggests that amplification effects can be much larger than predicted by the two-dimensional models. Relevant parameters are, by order of importance, source geometry, fault-to-source distance, fault length and position, and dip angle.

Our results show significant deviations from the predictions of IHMs. Differences can, in some cases, be more important than, for example, the effect from applying different source models, i.e. differences between solving

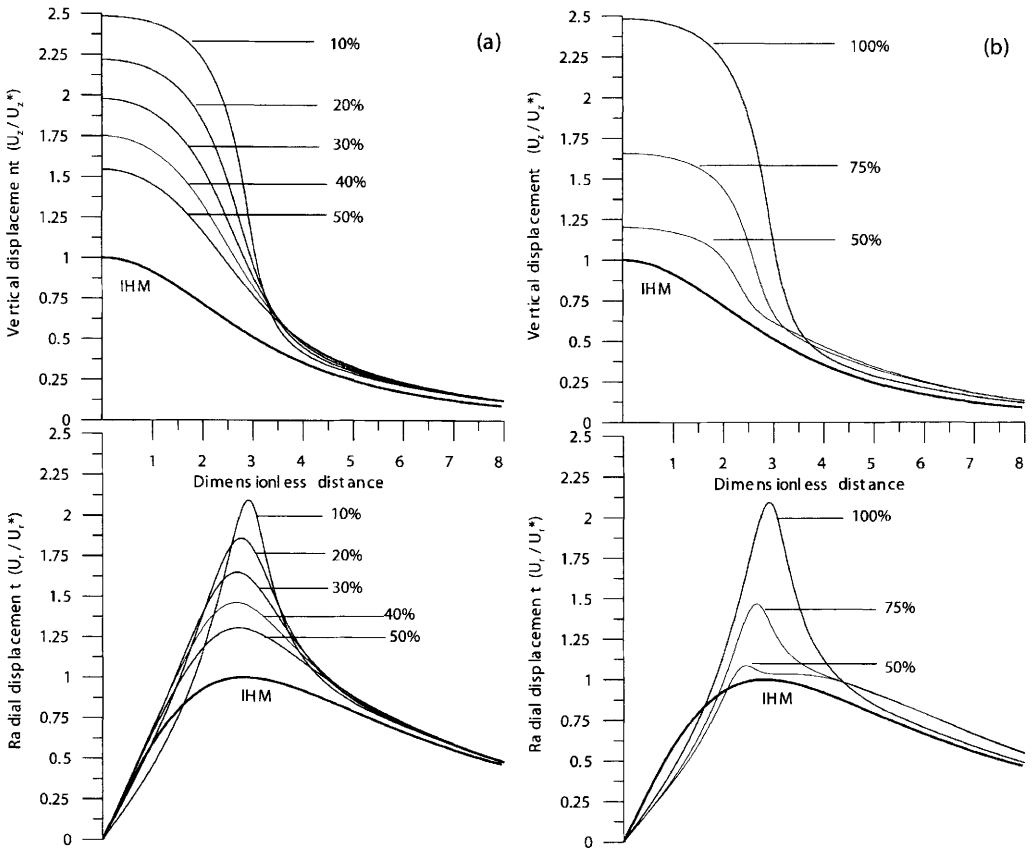

Fig. 4. (**a**) Effect of depth of fault on vertical (top) and radial (bottom) displacements. Results for faults starting at 10, 20, 30, 40 and 50% of the fault penetration depth. The corresponding fault lengths L_f are 3.7, 3.3, 2.9, 2.4 and 2 km approximately. Bold lines indicate the predictions of the IHM. Plots are normalized as explained in Figure 3. Results are obtained for $a=1$ km, $d=4$ km, $\varepsilon=4$, $\xi_f=2$, and $\alpha=15°$. (**b**) The same but with varying penetration depths. Results for faults penetrating to 100, 75 and 50% of the source depth. The corresponding fault lengths are 3.7, 2.7 and 1.7 km, respectively.

for point or finite sources (Dietrich & Decker 1975; McTigue 1987) or the effect from accounting for or omitting the influence of topography on ground deformation. Neglecting faults when fitting data at active calderas using either finite or point-like sources may lead to substantial errors for: (1) source location, due to the change in the spatial distribution of the degree of deformation, and/or (2) source size and pressure changes, due to the amplification of the absolute value of both vertical and horizontal deformation components. Relative errors are more pronounced for prolate and – to a lesser extent – spherical geometries. Linear elastic and visco-elastic models entail a linear positive relationship between pressure changes in the source and the resultant surface displacements. As a consequence, pressure changes may be overestimated by a factor of two to three in situations involving prolate and spherical source geometries. In contrast, relative errors for sill-like sources are likely to be of a second order, except in the vicinity of the fault projection to the surface, as we explore below.

Modelling results for periods of ground subsidence from analytical solutions that are not accounting for lateral discontinuities would suffer from equally distinct differences in the deduced subsurface volume/pressure changes, or poorer qualities of fit if compared to our solutions. Results obtained from elastic IHMs are often regarded with reservations, because they can provide unrealistic values for pressure change (Bonafede & Mazzanti 1998), and more complex models accounting, for example, for visco-elasticity, appear to provide more realistic values (Newman *et al.* 2001). However, deducing 'realistic' visco-elastic property values such as

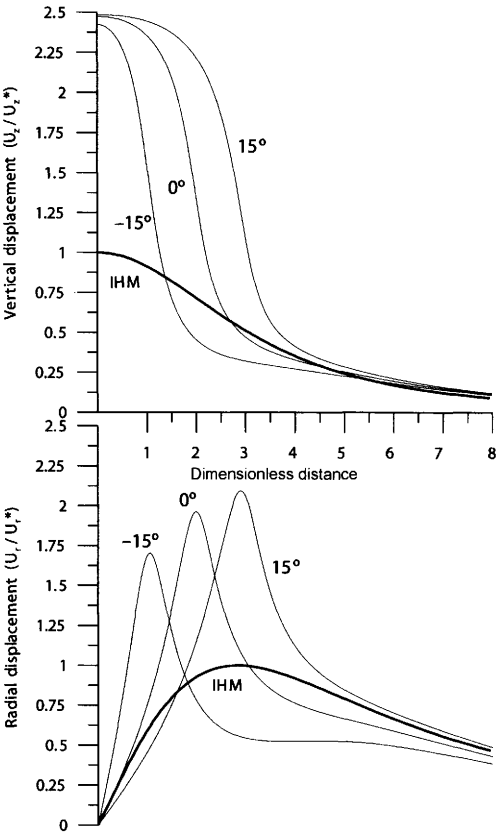

Fig. 5. Effect of fault inclination on vertical (top) and radial (bottom) displacements. Results are shown for faults with dip angles α of −15° (outward-dipping), 0°, and 15° (inward-dipping). Bold lines are the predictions of the IHM. Normalizations according to Figure 3. Results are obtained for $a=1$ km, $d=4$ km, $\varepsilon=4$, $\xi_f=2$, and $L_f=3725$ m.

structural relaxation times or the dimension of a visco-elastic halo around a magma reservoir is difficult and prone to large errors. Information about the presence of faults and an assessment of their geometry may, however, be obtained in a more straightforward way during detailed fieldwork or seismic studies (Mori & McKee 1987; Prejean *et al.* 2002). As a consequence, we would argue that modelling pressurized sources within the framework of elastic IHM may also provide physically realistic parameter values if structural discontinuities are accounted for.

Application of the model

In the previous sections, we performed a parametric study on the influence of faults on the deformation pattern at uplifting calderas. The two key findings were: (1) faults may significantly amplify ground deformation induced by pressurizing a subsurface source, resulting in a overestimation of associated pressure changes when solving the inverse problem by means of IHM and, (2) faults may distort the spatial deformation pattern, leading to an abrupt decline in uplift (large uplift/distance gradients) in proximity to faults. In this section, we present two natural examples, which highlight both of the key findings. It is important to note that our purpose is not provide a full quantitative solution and best-fit inversion for these two particular cases, but to illustrate qualitatively the theoretical findings for the natural examples.

Campi Flegrei, Italy

The Campi Flegrei caldera (CFc) resulted from two main collapse events (37 and 12 ka) and hosted a number of 'post-caldera' eruptions (Rosi *et al.* 1983; Orsi *et al.* 1996). Furthermore, it is renowned for its continuous ground deformation over the past 2000 years (Parascondola 1947). The 1.8-m non-eruptive uplift between 1982 and 1984 has led to a controversial debate as to the subsurface processes that cause the observed ground deformation: magma movement (Berrino *et al.* 1984) or hydrothermal fluid migration (Bonafede & Mazzanti 1998).

Gottsmann *et al.* (2006*b*) performed a coupled inversion of deformation and gravity data (Berrino *et al.* 1984) for the 1982–1984 uplift period, and proposed a prolate spheroid source undergoing a volume change of 71×10^6 m^3 as the best-fitting IHM solution. Density constraints from gravimetric data inversion allowed the authors to suggest a hybrid nature for the causative source, with both magmatic and hydrothermal components. In a follow-up paper (Gottsmann *et al.* 2006*a*) delineated the hybrid body via two vertically stacked spherical sources representing a deep magmatic and a shallow hydrothermal reservoir. The source parameters thus obtained are given in Table 1. A limitation of the analytical inversion result was that the shallow source (at 2 km depth) does not verify the point-source hypothesis. In order to overcome this drawback, the results were validated via a 3D finite-element model and, assuming a rigidity of 10 GPa, the authors deduced pressure increases of 33 and 42 MPa for the deep and the shallow source, respectively, which represent the maximum allowable pressure changes based on a realistic assessment of the tensile strengths of the encasing rocks. The presence of faults within the caldera (Orsi *et al.* 1996) suggests that their effect on the ground-deformation pattern should be taken into account, particularly in light of the

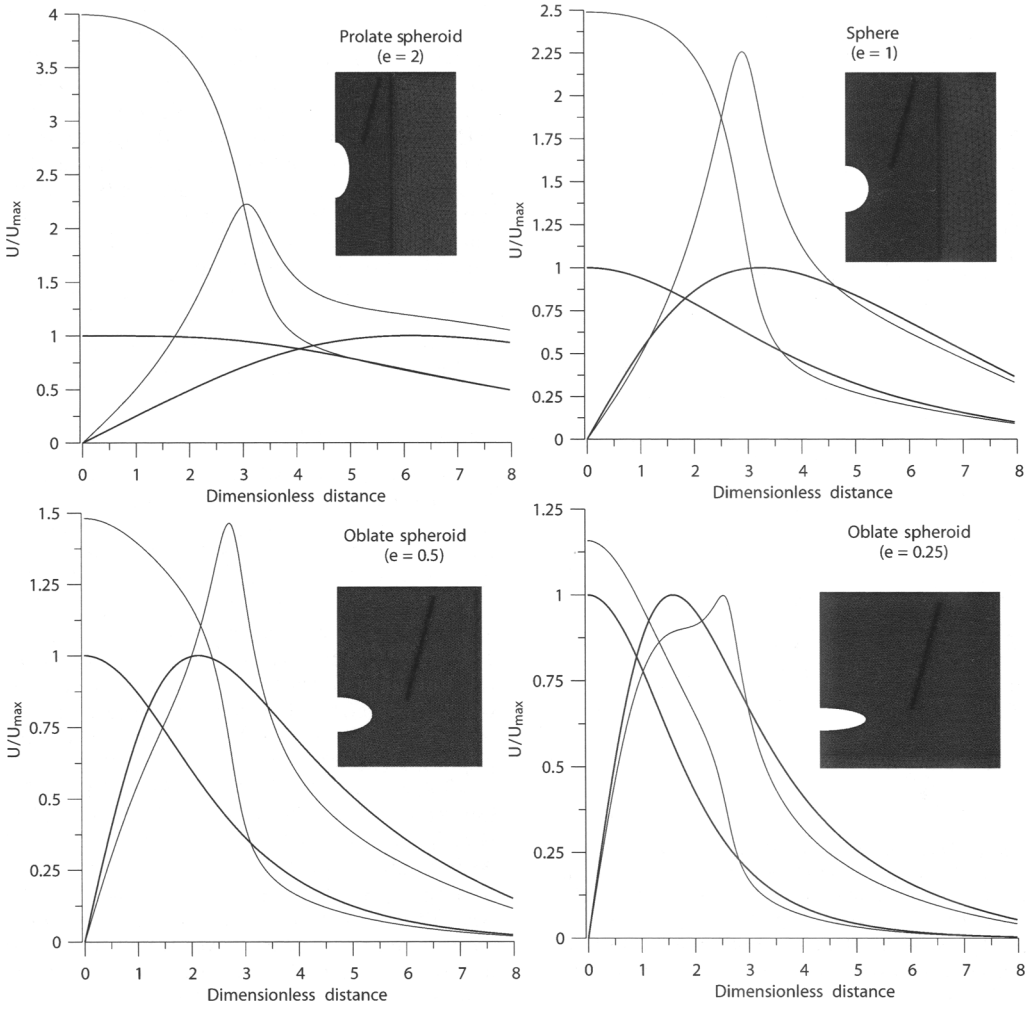

Fig. 6. Effect of source geometry and fault on surface deformation. Amplification of vertical and radial displacements for different spheroids of aspect ratios e (vertical to horizontal extension) equal to 2, 1, 0.5 and 0.25. All sources are fixed to equal volume. Details of the meshes around the sources are shown as insets. Results are normalized to the predictions of the IHM (bold lines). Note how the amplification is highly dependent on the source geometry. Model parameters for these solutions are $d=4$ km, $\varepsilon=4$, $\alpha=15°$, $\xi_f=2$ and $L_f=3725$ m.

mutual dependence of the inferred source geometries and faults on the stress field, as explained above.

We consider the effect of caldera faults for two different cases. Case 1 accounts for the caldera boundaries, and assumes a ring-fault with $r_f=5.5$ km ($\xi_f=4$), $d=4$ km, and $\alpha=15°$ ($L_f=4150$ m). Case 2 represents an approximation to the inner-caldera boundary fault (Beauducel *et al.* 2004) and considers $r_f=2.5$ km ($\xi_f=1.8$), $d=3.1$ km, and $\alpha=15°$ ($L_f=2070$ m). For simplification, axial symmetry and flat topography are assumed. Note, that we are here not aiming at providing a full-scale inversion of the data. Our intention here is to show that accounting for bounding faults at the CFc may provide acceptable values for overpressures assuming simple source geometries. Results are shown in Figure 7. In both cases we obtain best fits with values of 30 MPa for each source, i.e. with a decrease in the inferred pressure change of about 25% in the shallow source and 10% in the deeper source. Case 2 gives a better fit to the measured data.

A further important point when accounting for lateral discontinuities concerns

Table 1. *Source parameters of coupled gravity and deformation IHM inversion for two spherical sources during inflation (1982–1984) at the Campi Flegrei Caldera*

Variable	Source 1	Source 2
x (UTM)	426 300	426 500
y (UTM)	4 521 300	4 519 200
z (m)	5300	2000
ΔV (10^6 m^3)	26.7	32.6
α (m)	1286	1374
ρ (kg m^{-3})	3600	1400

Results from Gottsmann *et al.* (2006*b*). x and y are Easting (m) and Northing (m) positions of the centre of each source, z is depth of source centre, ΔV is volume change, a is source radius, and ρ is bulk density.

micro-gravimetric data obtained simultaneously with deformation data during caldera unrest. Contrary to their application in IHM inversions (Walsh & Rice 1979), measurements need to be corrected for Bouguer effects: i.e. coupling effects between gravity and elastic deformation (Bonafede & Mazzanti 1998). Accounting for these effects using a Bouguer density of 2000 kg m^{-3}, and correcting results from the gravimetric data inversion presented in Gottsmann *et al.* (2006*a*) requires an input of material with a density ρ of 2400 kg m^{-3} into the deep source, whereas the shallow pressure-dominated source undergoes a negligible mass input of material with $\rho = 400$ kg m^{-3}). A geologically plausible scenario is a recharge of magma at depth, coupling into a shallower hydrothermal system and inducing volume expansion of supercritical fluids. As such, the observed inflation may be interpreted to result from a combination of deep-seated magmatic and shallow hydrothermal processes. The total subsurface volume change of $60 \pm 2 \times 10^6$ m^3 is almost equally split between the two sources, and the associated gravity change is dominated by mass input into the deep source (Gottsmann *et al.* 2006*a*). Future uplift at the Campi Flegrei may be associated with subsurface magma recharge; however, we find that the hydrothermal system plays an important role during unrest at the CFc and the hazards associated with either source need to be assessed for risk mitigation.

Sierra Negra, Galapagos, Ecuador

Ground deformation of up to 2.7 m was detected at the Sierra Negra Caldera (Isabela Island) by interferometric synthetic aperture radar (InSAR) observations (Amelung *et al.* 2000; Jonsson *et al.* 2005). Although both spatially and temporally variable during this period, the deformation patterns in 1992–1997 and 1998–1999 were similar, with the maximum uplift located at the centre of the 7 × 10-km-wide caldera (Jonsson *et al.* 2005). Trapdoor faulting occurring along the southern part of the caldera between 1997 and 1998 was found to best explain the asymmetrical fringe pattern obtained during that time (Jonsson *et al.* 2005). In this section, we investigate the 1998–1999 caldera uplift during which a maximum line-of-sight (LOS) range change of 0.3 m was observed in the caldera centre (Figure 8a), subsequent to the faulting event. No significant ground displacement was detected beyond the caldera rim, which could suggest that the area affected by ground deformation may have been controlled by caldera ring-faults. With data available from only one ascending satellite orbit (LOS unit vector: (0.3790, 0.0806, –0.9219)) it is impossible to calculate the full 3D displacement field. We hence present all modelling results as LOS range change data.

Amelung *et al.* (2000) and Jonsson *et al.* (2005) inferred the presence of a growing sill from data inversion using an IHM, as the ovoid InSAR fringe pattern appeared inconsistent with, for example, a spherical source geometry. Using an entirely different approach (Yun *et al.* 2005) concluded that a pressurized diapir could fit the 1998–1999 data equally well. In fact, within reasonable limits of the required pressure increase, we find the displacement data to be relatively insensitive to the source geometry, as long as the source has a more or less flat surface and a lateral extent of 2–3 km. As an example, Figure 8 shows the fit obtained by a sill-like body with $d = 2$ km, $a = 2.5$ km and a thickness that decreases linearly from 200 m at the centre ($r = 0$) to 15 m at the end ($r = a$). The body overpressure is 1.5 MPa and the rigidity of the host rock is 10 GPa.

We find, however, that the particular deformation pattern observed along the southern edge of the caldera cannot be modelled adequately by either source geometry in an IHM. A stark distortion of the LOS data appears at a distance of *c.* 3 km from the maximum LOS amplitude (Fig. 8), with a large displacement/distance gradient similar to those obtained in our previous parametric study close to lateral discontinuities. Note that the southern part of the caldera has been the locus of trapdoor faulting in the year preceding the uplift considered here. A possible geological interpretation could be that this faulting episode has had a buttressing effect along the southern caldera margin, preventing surface displacement beyond the faulted area during

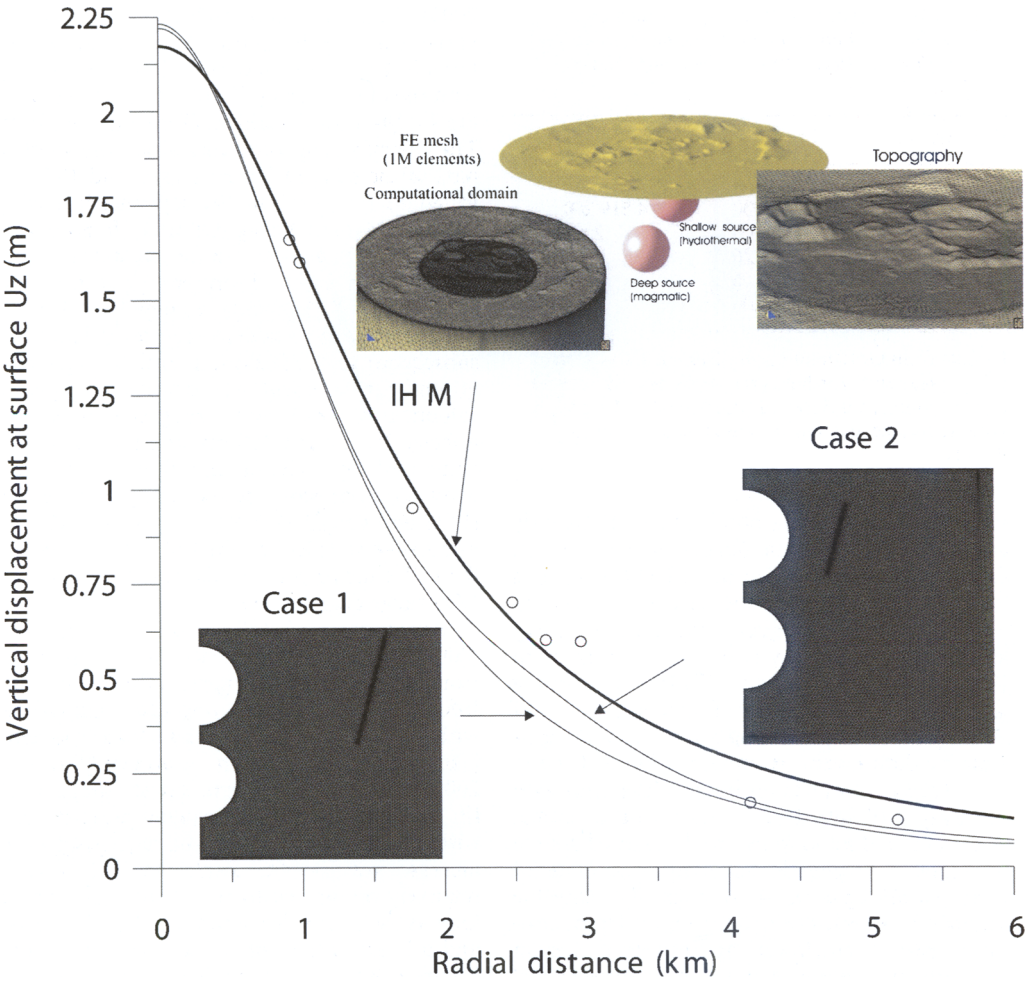

Fig. 7. Results obtained for uplift at CFc (1982–1984) for the two spherical sources reported in Table 1. Vertical displacements at surface *v*. radial distance from the centre of the shallow source. Circles indicate data from Berrino *et al.* (1984). The bold line is a result from 3D simulation using pressure increases of 42 and 33 MPa for the shallow and deep source, respectively (Gottsmann *et al.* 2006*a*) and ignoring the influence of faults. Cases 1 and 2 show results for two different fault geometries. Deduced source overpressures are 30 MPa in either source. Details of the finite-element meshes are shown for both cases.

subsequent continuing uplift. We can successfully model this distortion by accounting for a vertical discontinuity with $r_f = 3$ km ($\xi_f = 1.2$) and $L_f = 1.5$ km (see Figs 8c & 8d). The inclusion of a discontinuity represents a significant improvement of the quality of fit to the data as compared to the fit from a sill-like body using an IHM, yet, due to the sill-like geometry of the source, it does not imply any substantial reduction in the pressure change (1.5 MPa for the IHM solution when compared to 1.3 MPa deduced from this study). We note again that the main objective here is not to solve for the best 3D fit but to present a natural example that illustrates the significant distortion of the ground deformation pattern induced by the presence of faults.

Summary and conclusions

We have shown that structural discontinuities (ring faults or boundary faults) may significantly influence the deformation field at active calderas undergoing subsurface volume/pressure changes. Ignoring the effect of faults during the inversion of ground deformation data using IHMs may lead to a significant error in the deduced volume/

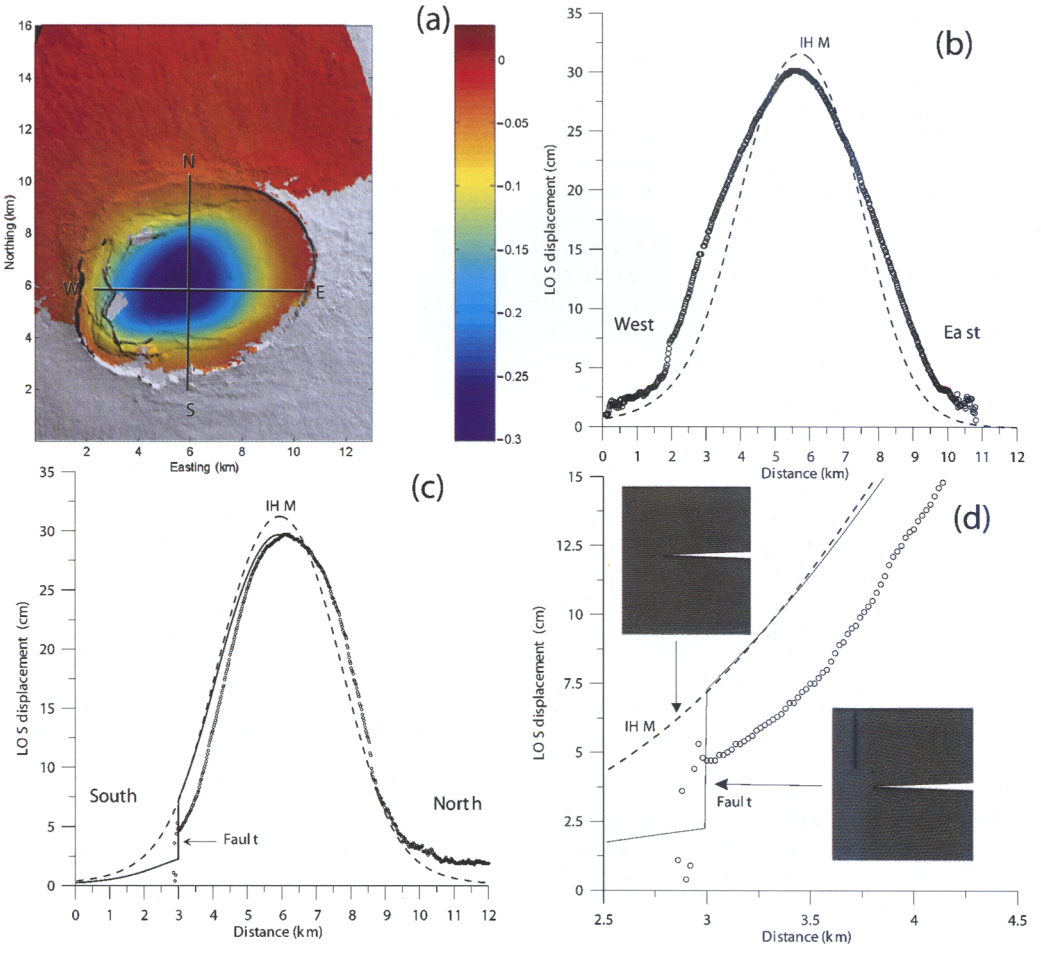

Fig. 8. (**a**) Observed InSAR LOS range change (in m) at Sierra Negra caldera for 1998–1999, draped over a digital elevation model. Data after Jonsson *et al.* (2005). B–D: profiles of LOS data from (**a**) and model fits. Observed data are indicated by circles. (**b**) east–west profile showing observed data and model fit (line) for the sill-like source geometry reported in Jonsson *et al.* (2005). The deduced pressure increase is 1.5 MPa (see text for details) without accounting for the fault (IHM). (**c**) north-south profile showing observed data, IHM fit and fit from accounting for a vertical fault with $L_f = 1$ km and $\xi_f = 1.2$. Resultant pressure change is 1.3 MPa. (**d**) close-up of lower left-hand corner of (**c**). Note how inclusion of a trapdoor fault in the model significantly improves the fit in the vicinity of the inferred fault by capturing the sharp change in the gradient of the displacement field. Details of the model geometries for the IHM and the fault model are also shown.

pressure changes. However, we find that the influence of faults on the deformation field is highly dependent on source geometry. Bodies such as sills or oblate spheroids are very effective in concentrating deformation directly above their upper surface, because the induced displacement vectors tend to be vertical. In contrast, spherical or prolate bodies distribute their displacement vectors predominantly non-vertically (i.e. in the direction normal to (sub)vertical ring faults) and thus require a significantly higher pressure increase than oblate geometries in order to trigger the same amount of surface displacement. As a consequence, the effect of faults on the displacement field becomes more pronounced for the latter geometries compared to the former. Boundary faults can significantly amplify ground displacement and distort the pattern, leading to abrupt changes in displacement/distance gradients in proximity to faults. We have presented two natural examples that illustrate each of these phenomena.

For the case of ground inflation at the Campi Flegrei Caldera (1982–1984) our approach has shown that despite using a simple two-spherical source model, accounting for lateral discontinuities provides physically realistic results for source parameter values. Considering two sources and accounting for faults, this uplift episode can be explained with overpressures in the range or lower than the expected strength of the rocks, even if a rather high value of 10 GPa is assumed for crust rigidity. In the case of post-faulting uplift at the Sierra Negra Caldera between 1998 and 1999, we find that particular surface displacement data observed with radar interferometry along the recently faulted southern caldera rim are very similar to deformation patterns proposed by our forward modelling results and can be best explained by an interaction of the displacement field caused by a flat-topped pressurized body with a lateral discontinuity. Satellite-based remote sensing of surface displacements at active caldera volcanoes can provide important data, particularly across caldera boundaries, where ground-based observation techniques often provide a limited resolution. Future analysis of such datasets will be an important test for the modelling concepts brought forward here.

Boundary faults play an important role in the evolution of caldera systems, as they provide pathways from deep magma reservoirs for magmatic gases (Farrar *et al.* 1995), as well as for magmatic intrusions (Saunders 2004). We conclude that coupling data inversion using IHM with numerical modelling and taking into account lateral structural discontinuities may provide important insights into the subsurface pressure/volume changes beneath restless caldera volcanoes. However, geodetic data alone cannot unambiguously resolve the subsurface kinetics of active volcanic systems, and data obtained from other monitoring techniques need to be taken into account (Cayol & Cornet 1998; Beauducel *et al.* 2000; Battaglia *et al.* 2003; Gottsmann *et al.* 2006*b*) to infer on source parameters and dynamics. Only then can the inversion of deformation data be confidently incorporated for the assessment of hazards at active volcanic areas.

AF was supported by the EU 'EXPLORIS' project (EVR1-CT-2002-40026). JG acknowledges support from a Ramon y Cajal grant by the Spanish Ministry of Science and a University Research Fellowship by the Royal Society of London. We are indebted to S. Jonsson and F. Amelung for providing InSAR data for Sierra Negra, and for their helpful comments. We thank L. Wooller for his views on an earlier draft of this manuscript, as well as two anonymous reviewers and the Associate Editor G. De Natale for constructive comments.

References

ACOCELLA, V., CIFELLI, F. & FUNICIELLO, R. 2000. Analogue models of collapse calderas and resurgent domes. *Journal of Volcanology and Geothermal Research*, **104**, 81–96.

AMELUNG, F., JONSSON, S., ZEBKER, H. & SEGALL, P. 2000. Widespread uplift and 'trapdoor' faulting on Galapagos volcanoes observed with radar interferometry. *Nature*, **407**, 993–996.

BATTAGLIA, M., ROBERTS, C. & SEGALL, P. 1999. Magma intrusion beneath Long Valley caldera confirmed by temporal changes in gravity. *Science*, **285**, 2119–2122.

BATTAGLIA, M., SEGALL, P. & ROBERTS, C. 2003. The mechanics of unrest at Long Valley caldera, California. 2. Constraining the nature of the source using geodetic and micro-gravity data. *Journal of Volcanology and Geothermal Research*, **127**, 219–245.

BEAUDUCEL, F., CORNET, F., SUHANTO, E., DUQUESNOY, T. & KASSER, M. 2000. Constraints on magma flux from displacements data at Merapi volcano. *Journal of Geophysical Research*, **105**, 8193–8204.

BEAUDUCEL, F., DE NATALE, G., OBRIZZO, F. & PINGUE, F. 2004. 3-D modelling of Campi Flegrei ground deformations: role of caldera boundary discontinuities. *Pure and Applied Geophysics*, **161**, 1329–1344.

BERRINO, G., CORRADO, G., LUONGO, G. & TORO, B. 1984. Ground deformation and gravity changes accompanying the 1982 Pozzuoli uplift. *Bulletin of Volcanology*, **47**, 188–200.

BONAFEDE, M. 1990. Axisymmetric deformation of a thermo-poro-elastic half-space: inflation of a magma chamber. *Geophysical Journal International*, **103**, 289–299.

BONAFEDE, M. & MAZZANTI, M. 1998. Modelling gravity variations consistent with ground deformation in the Campi Flegrei caldera (Italy). *Journal of Volcanology and Geothermal Research*, **81**, 137–157.

CAYOL, V. & CORNET, F. H. 1998. 3D modelling of the 1983–1984 eruption at Piton de la Fournaise volcano, Reunion Island, Indian Ocean. *Journal of Geophysical Research*, **103**, 18 025–18 037.

CODINA, R. & FOLCH, A. 2004. A stabilized finite element predictor–corrector scheme for the incompressible Navier–Stokes equations using a nodal-based implementation. *International Journal of Numerical Methods in Fluids*, **44**, 483–503.

DAVIS, P. M. 1986. Surface deformation due to inflation of an arbitrarily oriented triaxial ellipsoidal cavity in an elastic half-space, with reference to Kilauea volcano, Hawaii. *Journal of Geophysical Research*, **91**, 7429–7438.

DE NATALE, G. & PINGUE, F. 1993. Ground deformations in collapsed caldera structures. *Journal of Volcanology and Geothermal Research*, **57**, 19–38.

DE NATALE, G., PETRAZZUOLI, S. & PINGUE, F. 1997. The effect of collapse structures on ground deformation in calderas. *Geophysical Research Letters*, **24**, 1555–1558.

DIETRICH, J. H. & DECKER, R. W. 1975. Finite element modeling of surface deformation associated with volcanism. *Journal of Geophysical Research*, **80**, 4094–4106.

DRAGONI, M. & MAGNANENSI, C. 1989. Displacement and stress produced by a pressurized, spherical magma chamber, surrounded by a viscoelastic shell. *Physics of the Earth and Planetary Interiors*, **56**, 316–328.

FARRAR, C. D., SOREY, M. L. *ET AL.* 1995. Forest-killing diffuse CO_2 emission at Mammoth Mountain as a sign of magmatic unrest. *Nature*, **376**, 675–678.

FERNANDEZ, J., RUNDLE, J. B., GRANELL, R. D. R. & YU, T. T. 1997. Programs to compute deformation due to a magma intrusion in elastic-gravitational layered Earth models. *Computers and Geosciences*, **23**, 231–249.

FIALKO, Y., KHAZAN, Y. & SIMONS, M. 2001. Deformation due to a pressurized horizontal circular crack in an elastic half-space, with applications to volcano geodesy. *Geophysical Journal International*, **146**, 181–191.

FOLCH, A., FERNANDEZ, J., RUNDLE, J. B. & MARTÍ, J. 2000. Ground deformation in a viscoelastic medium composed of a layer overlying a half space. A comparison between point and extended sources. *Geophysical Journal International*, **140**, 37–50.

GOTTSMANN, J., FOLCH, A. & RYMER, H. 2006*a*. Caldera unrest at Campi Flegrei: a contribution to the magmatic vs. hydrothermal debate from inverse and finite element modeling. *Journal of Geophysical Research*, in press.

GOTTSMANN, J., RYMER, H. & BERRINO, G. 2006*b*. Caldera unrest at the Campi Flegrei: a critical evaluation of source parameters from geodetic data inversion. *Journal of Volcanology and Geothermal Research*, **150**, 132–145.

GUDMUNDSSON, A., MARTÍ, J. & TURON, E. 1997. Stress field generating ring faults in volcanoes. *Geophysical Research Letters*, **24**, 1559–1562.

HOFTON, M. A., RUNDLE, J. B. & FOULGER, G. R. 1995. Horizontal surface deformation due to dike emplacement in an elastic–gravitational layer overlying a viscoelastic–gravitational half-space. *Journal of Geophysical Research*, **100**, 6329–6338.

JONSSON, S., ZEBKER, H. & AMELUNG, F. 2005. On trapdoor faulting at Sierra Negra volcano, Galapagos. *Journal of Volcanology and Geothermal Research*, **144**, 59–71.

LIPMAN, P. 2000. Calderas. *In*: SIGURDSSON, H., HOUGHTON, B. F., MCNUTT, S. R., RYMER, H. & STIX, J. (eds) *Encyclopedia of Volcanoes*. Academic Press, San Diego, 643–662.

MCTIGUE, D. 1987. Elastic stress and deformation near a finite spherical magma body: Resolution of the point source paradox. *Journal of Geophysical Research*, **92**, 12 931–12 940.

MOGI, K. 1958. Relations between eruptions of various volcanoes and the deformations of the ground surfaces around them. *Bulletin of the Earthquake Research Institute*, **36**, 99–134.

MORI, J. & MCKEE, C. 1987. Outward-dipping ring-fault structure at Rabaul caldera as shown by earthquake locations. *Science*, **235**, 193–195.

MURPHY, M. D. SPARKS, R. J. S. *ET AL.* 1998. The role of magma mixing in triggering the current eruption at the Soufriere Hills volcano, Montserrat. *Geophysical Research Letters*, **25**, 3433–3436.

NEWHALL, C. G. & DZURISIN, D. 1988. *Historical Unrest at Large Calderas of the World*. US Geological Survey Bulletin US, 1855. Geological Survey, Reston, VA.

NEWMAN, A. V., DIXON, T. H., OFOEGBU, G. I. & DIXON, J. E. 2001. Geodetic and seismic constraints on recent activity at Long Valley caldera, California: evidence for viscoelastic rheology. *Journal of Volcanology and Geothermal Research*, **105**, 183–206.

ORSI, G., DE VITA, S. & DI VITO, M. 1996. The restless, resurgent Campi Flegrei nested caldera (Italy): constraints on its evolution and configuration. *Journal of Volcanology and Geothermal Research*, **74**, 179–214.

PARASCONDOLA, A. 1947. *I fenomeni bradisismici del Sarapeo di Pozzuoli*. Genovese, Naples.

PREJEAN, S., ELLSWORTH, W., ZOBACK, M. & WALDHAUSER, F. 2002. Fault structure and kinematics of the Long Valley caldera region, California, revealed by high-accuracy earthquake hypocenters and focal mechanism stress inversions. *Journal of Geophysical Research*, **107**(B12), 2355.

ROSI, M., SBRANA, A. & PRINCIPE, C. 1983. The Phlegraean Fields: structural evolution, volcanic history and eruptive mechanisms. *Journal of Volcanology and Geothermal Research*, **17**, 273–288.

SAUNDERS, S. J. 2004. The possible contribution of circumferential fault intrusion to caldera resurgence. *Bulletin of Volcanology*, **67**, 57–71.

WALSH, J. B. & RICE, J. R. 1979. Local changes in gravity resulting from deformation. *Journal of Geophysical Research*, **84**, 156–170.

YANG, X. M., DAVIS, P. & DIETRICH, J. H. 1988. Deformation from inflation of a dipping finite prolate spheroid in an elastic half-space as a model for volcanic stressing. *Journal of Geophysical Research*, **93**, 4249–4257.

YUN, S., SEGALL, P. & ZEBKER, H. 2005. Constraints on magma chamber geometry at Sierra Negra volcano, Galapagos Islands, based on InSAR observations. *Journal of Volcanology and Geothermal Research*, **150**, 232–243.